The British University in Egypt
BUE Scholar

Mechanical Engineering | Engineering

2022

Implementation of multiscale mechanisms in finite element analysis of active composite structures

Amany G. Micheal Prof.
The British University in Egypt, amany.micheal@bue.edu.eg

Yehia Bahei-El-Din
The British University in Egypt, ybahei@bue.edu.eg

Follow this and additional works at: https://buescholar.bue.edu.eg/mech_eng

 Part of the Engineering Mechanics Commons, and the Other Materials Science and Engineering Commons

Recommended Citation

Micheal, Amany G. Prof. and Bahei-El-Din, Yehia, "Implementation of multiscale mechanisms in finite element analysis of active composite structures" (2022). *Mechanical Engineering*. 10.
https://buescholar.bue.edu.eg/mech_eng/10

This Article is brought to you for free and open access by the Engineering at BUE Scholar. It has been accepted for inclusion in Mechanical Engineering by an authorized administrator of BUE Scholar. For more information, please contact bue.scholar@gmail.com.

Check for updates

Review

JOURNAL OF COMPOSITE MATERIALS

Journal of Composite Materials
2022, Vol. 56(13) 2129–2144
© The Author(s) 2022
Article reuse guidelines:
sagepub.com/journals-permissions
DOI: 10.1177/00219983221082492
journals.sagepub.com/home/jcm
SAGE

Implementation of multiscale mechanisms in finite element analysis of active composite structures

Amany Micheal and Yehia A Bahei-El-Din

Abstract

Interrogation of composite structures for inherent damage is investigated implementing three-tier analysis scheme. The analysis starts at the structure level where a general-purpose Finite Element code ABAQUS is employed to obtain the stress field in the second level of analysis that is the composite laminate. A special material routine is prepared to propagate the local fields to the individual plies and hence to the third level of analysis which is the microstructure modelling of the composite. Through the third level of analysis, interface damage between fiber and matrix is checked implementing a certain failure criteria. The interaction between the different length scales; that are, structure, macro, and micro scales, is implemented using the non-mechanical strains caused by damage. Embedment of electrically active fibers in the laminate serves as a tool to interrogate the structure for inherent damage through the electric displacement generated due to the electro-mechanical coupling. To verify the developed multi-scale model, a comparison with the experimental results of a tube problem under combined internal pressure and axial load is presented. The results show good agreement in both the undamaged and damaged state. As an application, a plate with a hole under biaxial load is solved. The output includes not only the structure global behavior during damage but also detailed information about the location of damage within the structure, the plies that exhibit damage, type of damage and the fiber/matrix debonded length. Comparison between the electric displacement of the active fibers in the undamaged and damaged states is presented as well.

Keywords

composite structures, finite elements, multiscale, piezo/pyro-electricity, damage

Introduction

Piezoelectric materials have been used as both sensors and actuators for smart structures. They may be used for structural health monitoring (SHM) or for control of deformation purposes. In applications where this functionality together with load carrying capacity for a certain application are desired, piezoelectric filaments are embedded in a polymeric matrix to form an electroactive unidirectional composite, which may be utilized in various laminated or woven architectures. Research in electrically active composites has seen both modeling and experimental efforts. In one class of work the focus has been on prediction of the overall properties of piezoelectric composites, including mechanical, electrical and coupled effects, particularly within the micromechanics framework. This is found, for example, in the work of Aboudi,[1] Berger et al.,[2,3] Chen,[4] and Della and Shu,[5] among others.

Detection of damage in composites using piezoelectricity has, on the other hand, seen extensive experimental work with a variety of methods, but a rather limited analytical work. The experimental methods have focused mainly on detection of damage in structures, or parts of structures using surface mounted piezoelectric wafers and embedded sensors, which are employed as both transmitters and receivers to interrogate structures for internal changes. This can be found, for example, in the work of Giurgiutiu and Soutis,[6] Li et al.,[7] Medeiros et al.[8,9] and Shivakumar.[10] Health monitoring of composites and laminates using embedded piezoelectric sensors can be found in the work of Cook,[11] De Medeiros et al.,[12] Hwang,[13] Katunin et al.,[14] Lissenden et al.,[15] Qing et al.,[16] Stojic et al.,[17] Verijenko

Center for Advanced Materials, The British University in Egypt, El-Shorouk City, Egypt

Corresponding author:
Amany Micheal, Center for Advanced Materials, The British University in Egypt, Cairo Suez Road, El-Shorouk City 11837, Egypt.
Email: Amany.micheal@bue.edu.eg

et al.[18] The trade-off between integrating active fibers into composite laminates and surface mounted PZT wafers for health monitoring was investigated in the work of Bruner et al.[19] Of principal concern is the effect of the sensors applied in the two methodologies on the overall mechanical properties, frequency tuning, and long-term monitoring.

Modeling damage in composites, including assessment of damage using analytical and/or computational tools can be found in the literature with different approaches. One of the promising schemes is the multi scale technique. A tri-scale damage analysis can be found in the work of Massarwa et al.[20] They developed a combined FE and High Fidelity Generalized Method of Cells (HFGMC) micro-mechanics solution for a composite structure including damage analysis. They integrated failure criteria which when satisfied, the failed elements are evacuated. Dinh et al.[21] analyzed laminates with inherent damage on the meso scale to investigate their behavior under bending and axial load. Expanding the finite element formulation to account for multiscale analysis can be found in the work of Ren et al.[22] Application of the multiscale analysis including plasticity and damage for composite laminate under low velocity impact can be found in the work of Singh et al.[23]

In this work, the Transformation Field Analysis (TFA) technique first presented by Dvorak[24] and Dvorak and Benveniste[25] was further developed to include non-mechanical stress and strain fields stemming from those released due to damage, as well as the fields caused by electromechanical coupling in electroactive constituents. Modeling of damage in inactive composites on micromechanical scale can be found in the work of Bahei-El-Din and Botros[26] and Bahei-El-Din et al.[27] Analysis of electrically active composites in both un-damaged and damaged state can be found in Bahei-El-Din[27] for 3D woven composites, Bahei-El-Din and Micheal[28] for pyro/piezoelectric composites. Bahei-El-Din and Micheal[29] and Micheal and Bahei-El-Din[30] studied the damage fibrous laminates with some/all electrically active plies. In Bahei-El-Din and Micheal,[31] the analysis scale escalated to laminated structures. Although the latter research modeled electroactive composite structures with a complex geometry, it stopped short of modeling damage initiation and assessment. For piezo-electric composites and laminates, TFA scheme yields a multiscale model leading to evaluating the effective electric permittivity in PZT fibers embedded in a damaged composite and assessment of the effect of damage progression on the electric displacement.

In this paper, the TFA scheme developed for electrically active composite structures developed by Bahei-El-Din and Micheal[31] is extended to model damage. This is a three-tier analysis; structural, macroscopic, and microscopic, which interact together and fields information flows between the three levels in both directions. Stress and strain transformation factors and concentration matrices of the modeled micro-structure and laminated macrostructure overall properties are computed in a preprocessing operation and stored for subsequent recall by the multiscale analysis. For composite structures with complex geometries, the analysis is performed within the finite element framework ABAQUS. The resulting stresses and strains on structural scale are applied back to the TFA analysis of composites and laminates in a post-processing operation to provide information on the state of damage in terms of the electric response of piezoelectric fibers.

The paper is organized as follows: in *Scales governing equations*, the governing equations of each scale analysis are presented. In *Damage analysis*, damage criteria for the composite microstructure level are presented and the strategy to evaluate the additional strain due to damage for both the composite and the laminate levels is illustrated. Clarification of the implementation of the embedded electrically active fibers is to sense damage is also given. *Solution strategy* is assigned to the solution phases; pre-processing, processing, and post-processing phases, and what operations to be performed on each scale in each phase. Applications are presented in *Application*; the first application is a tube problem under combined axial load and internal pressure. The results of the developed technique are compared with the experimental results available in the literature. The second application is a square plate with a concentric hole. The plate is a quasi-isotropic laminate with electrically active fibers and subjected to bi-axial load. Plots for the state of damage in each ply at different location of the plate are presented. Also, the effect of damage on the load-deformation curve of the structure and the electrical displacement in the active fibers are displayed.

Scales governing equations

A numerical technique is evolved to implement three-tier analysis for composite structures. The analysis escalates from the composite level to the laminate scale and then to a composite structure level. These levels interact together and the ordering of analysis goes both upward and downward. In this section, the governing equations that relate to each standalone scale are presented.

Composite level

Geometry. For the composite, the fibers are arranged in a certain pattern within the matrix such that a representative volume element, RVE, can be selected which when repeated periodically, the whole behavior of the composite can be estimated. The RVE is discretized into Q subvolumes in which the micromechanical fields are piecewise uniform and solved using finite element. There are many periodic fiber arrangements in the literature which include the square arrangement, rhombic arrangement and the periodic hexagonal array (PHA). The latter is adopted in this work.

Governing equations. The stress/strain field $\boldsymbol{\sigma}_r/\boldsymbol{\varepsilon}_r$ in any subvolume r, where $r = 1,2,..\ Q$, can be deduced from the composite overall stresses/strains $\overline{\boldsymbol{\sigma}}/\overline{\boldsymbol{\varepsilon}}$ using certain concentration factors. Under any load combinations, any subvolume s may exhibit non-mechanical fields, denoted as the Transformation Fields, that cannot be retrieved during unloading, that is, thermal, electrical, damage…etc. These transformation fields or eigenstresses/eigenstrains $\boldsymbol{\lambda}_s/\boldsymbol{\mu}_s$ affect the other subvolume r stress/strain fields using influence functions. To evaluate this effect, the Transformation Field Analysis (TFA) is implemented. This can be written as follows, Dvorak[24]

$$\boldsymbol{\varepsilon}_r = \boldsymbol{A}_r\overline{\boldsymbol{\varepsilon}} + \sum_{s=1,Q}\boldsymbol{D}_{rs}\boldsymbol{\mu}_s \tag{1}$$

$$\boldsymbol{\sigma}_r = \boldsymbol{B}_r\overline{\boldsymbol{\sigma}} + \sum_{s=1,Q}\mathbf{F}_{rs}\boldsymbol{\lambda}_s. \quad r,s = 1,Q \tag{2}$$

where $\boldsymbol{A}_r$, $\boldsymbol{B}_r$ are the strain and the stress concentration factors and $\mathbf{D}_{rs}$ and $\mathbf{F}_{rs}$ are influence functions for strain and stress, respectively. These factors are connected using the following identities[25]

$$\sum_{s=1,Q}c_r\boldsymbol{A}_r = \boldsymbol{I}, \quad \sum_{s=1,Q}c_r\boldsymbol{B}_r = \boldsymbol{I}, \quad \boldsymbol{A}_r\boldsymbol{M} = \boldsymbol{M}_r\boldsymbol{B}_r. \tag{3}$$

$$\sum_{s=1,Q}c_r\boldsymbol{F}_{rs} = \boldsymbol{0}, \quad \sum_{s=1,Q}c_r\boldsymbol{D}_{rs} = \boldsymbol{0}, \quad r = 1,Q \tag{4}$$

where c_r is the volume fraction of subvolume r, $\boldsymbol{M}$,$\boldsymbol{M}_r$ are the compliance of the composite and phase r, respectively. Closed forms for these functions are available using averaging models,[25] while in Finite Element solution, a certain technique is used to get the TFA variables depicted in equations (1) and (2) as will be discussed later.

Lamina constitutive equations. For a composite lamina with r subvolumes, the lamina stress and strain $\overline{\boldsymbol{\sigma}}$ and $\overline{\boldsymbol{\varepsilon}}$ are related in terms of the local stiffness and compliance matrices, $\overline{\boldsymbol{L}}$ and $\overline{\boldsymbol{M}}$, respectively, where the upper dash refers to the local coordinates system of the lamina. This can be written as follows[25]

$$\overline{\boldsymbol{\sigma}} = \overline{\boldsymbol{L}}\overline{\boldsymbol{\varepsilon}} + \overline{\boldsymbol{\lambda}}, \quad \overline{\boldsymbol{\varepsilon}} = \overline{\boldsymbol{M}}\overline{\boldsymbol{\sigma}} + \overline{\boldsymbol{\mu}} \tag{5}$$

where $\overline{\boldsymbol{L}}$ and $\overline{\boldsymbol{M}}$ can be evaluated from the counterpart r subvolumes stiffness and compliance $\boldsymbol{L}_\mathrm{r}$ and $\boldsymbol{M}_\mathrm{r}$ and volume fraction c_r as follows[29]

$$\boldsymbol{L} = \sum_{r=1,Q}c_r\boldsymbol{L}_r\boldsymbol{A}_r, \quad \overline{\boldsymbol{M}} = \sum_{r=1,Q}c_r\boldsymbol{M}_r\boldsymbol{B}_r. \tag{6}$$

The lamina eigenstress/eigenstrain, $\overline{\boldsymbol{\lambda}}/\overline{\boldsymbol{\mu}}$, can be expressed in terms of their counterpart of the subvolumes as follows[24]

$$\overline{\boldsymbol{\lambda}} = \sum_{r=1,Q}c_r\boldsymbol{A}_r^T\boldsymbol{\lambda}_r \tag{7}$$

$$\overline{\boldsymbol{\mu}} = \sum_{r=1,Q}c_r\boldsymbol{B}_r^T\boldsymbol{\mu}_r. \tag{8}$$

Laminate level

For the second tier of analysis which represents a laminate of n plies, the conventional laminate theory is employed in conjunction with the TFA model to consider the non-recoverable or the eigen fields. For any laminate with thickness h under in-plane normal and shear stress vector $\boldsymbol{\sigma}$ as shown in Figure 1, the strain in the mid plane $\boldsymbol{\varepsilon}_o$ can be expressed as summation of the effect of the mechanical stress $\boldsymbol{\sigma}$ and the eigen fields as follows[33]

$$\boldsymbol{\varepsilon}_o = h\boldsymbol{\mathcal{A}}'\boldsymbol{\sigma} + \boldsymbol{f}'. \tag{9}$$

where

$$\boldsymbol{\mathcal{A}}' = (I - \boldsymbol{\mathcal{B}}\mathcal{B})\boldsymbol{\mathcal{A}}^{-1},\ \boldsymbol{\mathcal{B}}' = -\boldsymbol{\mathcal{A}}^{-1}\boldsymbol{\mathcal{B}}\boldsymbol{\mathcal{D}}',\ \boldsymbol{\mathcal{C}}' = -\boldsymbol{\mathcal{D}}\boldsymbol{\mathcal{C}}\boldsymbol{\mathcal{A}}^{-1},\ \boldsymbol{\mathcal{D}}' = \left[\boldsymbol{\mathcal{D}} - \boldsymbol{\mathcal{B}}\boldsymbol{\mathcal{A}}^{-1},\boldsymbol{\mathcal{B}}\right]^{-1} \tag{10}$$

$\boldsymbol{\mathcal{A}},\boldsymbol{\mathcal{B}},\boldsymbol{\mathcal{D}}$ are related to the individual lamina i thickness t_i, the stiffness matrix in the laminate global coordinate system $\widehat{\boldsymbol{L}}_i$ and its distance from the mid plane of the laminate in the X_3 direction, $\mathbf{x}_3^i$ as follows[33]

$$\boldsymbol{\mathcal{A}} = \sum_{i=1,n}t_i\widehat{\boldsymbol{L}}_i, \boldsymbol{\mathcal{B}} = \sum_{i=1,n}\left(t_i\mathbf{x}_3^i\right)\widehat{\boldsymbol{L}}_i, \boldsymbol{\mathcal{D}} = \sum_{i=1,n}t_i\left(\frac{1}{12}t_i^2 + \mathbf{x}_3^{i^2}\right)\widehat{\boldsymbol{L}}_i. \tag{11}$$

The mid plane eigenstrain $\boldsymbol{f}'$ in equation (9) is related to the eignstresses of the individual plies, $\boldsymbol{\lambda}_i$, as follows

$$\boldsymbol{f}' = -\boldsymbol{\mathcal{B}}'\boldsymbol{g} - \boldsymbol{\mathcal{A}}'\boldsymbol{f}. \tag{12}$$

where

$$\boldsymbol{f} = \sum_{i=1,n}t_i\boldsymbol{\lambda}_i,\ \boldsymbol{g} = \sum_{i=1,n}\left(t_i\mathbf{x}_3^i\right)\boldsymbol{\lambda}_i. \tag{13}$$

On the other hand, the individual lamina i stress $\widehat{\boldsymbol{\sigma}}_i$, in terms of laminate stress $\widehat{\boldsymbol{\sigma}}$ and self-induced or other ply j eignstresses $\widehat{\boldsymbol{\lambda}}_j$ can be written as follows[33]

$$\widehat{\boldsymbol{\sigma}}_i = P_i\widehat{\boldsymbol{\sigma}} + \sum_{j=1,n}\boldsymbol{U}_{ij}\widehat{\boldsymbol{\lambda}}_j. \tag{14}$$

where $\boldsymbol{P}_i$ and $\boldsymbol{U}_{ij}$ are the distribution factor and influence function of lamina i, respectively. They are related to laminate/lamina properties as follows

$$\boldsymbol{P}_i = \widehat{\boldsymbol{L}}_i(\boldsymbol{\mathcal{A}}' + z_i\boldsymbol{\mathcal{C}}'), \tag{15}$$

$$\boldsymbol{U}_{ij} = \delta_{ij}\boldsymbol{I} - t_j\boldsymbol{P}_i. \tag{16}$$

Structure level

For a homogeneous material under the effect of uniform stresses and discretized into an assembled of finite volume elements V_m,$m = 1, 2,...\boldsymbol{M}$, piecewise uniform stress fields can be assumed within each element. Following the initial strain formulation by Zienkiewicz and Cormeau,[34] the stress field can be initially written in terms of the strain field as follows[35]

$$\boldsymbol{\sigma}_m = \boldsymbol{L}_m\boldsymbol{\varepsilon}_m^e = \boldsymbol{L}_m(\boldsymbol{\varepsilon}_m - \boldsymbol{\mu}). \tag{17}$$

where $\boldsymbol{L}_m$ is the elastic stiffness matrix of the material and $\boldsymbol{\mu}$ is any other non-mechanical field of strains that are non-recoverable such as thermal, electrical, damage…etc.

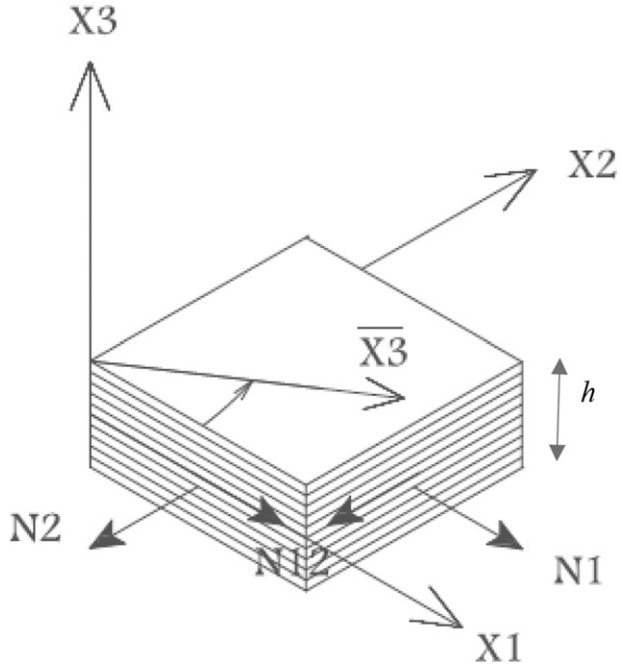

Figure 1. Laminate geometry and loading.

The resulting displacement field $\boldsymbol{u}_m$ in the subvolume V_m can be written as shape function of the coordinates of the nodes $\mathbf{a}_m$ that contribute in the subvolume V_m

$$\boldsymbol{u}_m = \boldsymbol{N}_m\,\boldsymbol{a}_m, \boldsymbol{N}_m = \left[\boldsymbol{N}_i\boldsymbol{N}_j\right]. \tag{18}$$

The strain field in the subvolume V_m can be written as function of the nodal displacement in the Cartesian coordinate system as follows

$$\boldsymbol{\varepsilon}_{ij} = \frac{1}{2}\left(\partial\boldsymbol{u}_i/\partial\mathbf{x}_i + \partial\boldsymbol{u}_j/\partial\mathbf{x}_j\right). \tag{19}$$

Substituting for the displacement field $\mathbf{u}_m$ in equation (19) with the nodal displacement shape function in equation (18), the above strain–displacement relationship can be rewritten as a linear differential operator such that

$$\boldsymbol{\varepsilon}_m = \boldsymbol{S}\,\boldsymbol{u}_{\mathrm{m}} = \boldsymbol{S}\boldsymbol{N}_m\,\boldsymbol{a}_m = \boldsymbol{\Lambda}_m\boldsymbol{a}_{\boldsymbol{a}}\,, \boldsymbol{\Lambda}_m = \left[\boldsymbol{\Lambda}_i^m\boldsymbol{\Lambda}_j^m\right] = \boldsymbol{S}\boldsymbol{N}_m. \tag{20}$$

If the strain field $\boldsymbol{\varepsilon}_m$ is assumed to be piecewise uniform within the subvolume element V_m, the shape function $\boldsymbol{N}_m$ is required to be linear and the coefficient matrix $\boldsymbol{\Lambda}_m$ is constant.

For the case of no body force, the traction at the nodes of any subvolume V_m can be written as the volume integration of the stress within this element as follows

$$\boldsymbol{q}_m = \int_{V_m} \boldsymbol{\Lambda}_m^{\mathrm{T}}\,\boldsymbol{\sigma}_m \mathrm{dV}_m \tag{21}$$

Substituting equation (17) into equation (21) and considering the strain–displacement relation given in equation (20), the equivalent nodal forces at any given sub-volume can be written follows

$$\boldsymbol{q}_i^m = \sum_{j=i}^{P} \boldsymbol{q}_{ij}^m\boldsymbol{a}_j^m + \boldsymbol{f}_i^m. \tag{22}$$

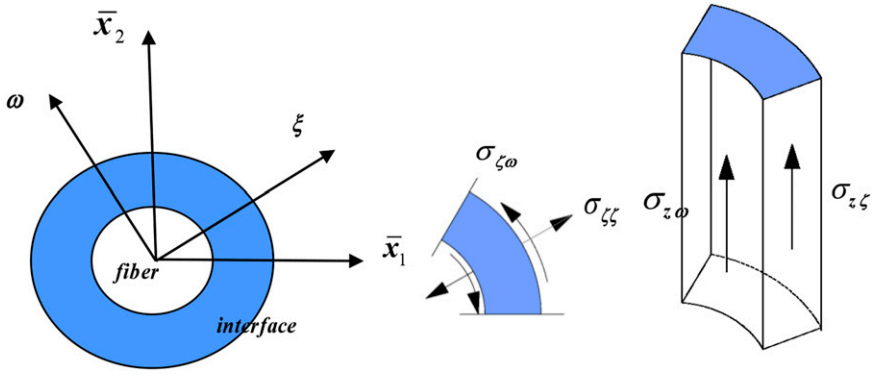

Figure 2. Fiber/Matrix interface stresses in polar coordinates.

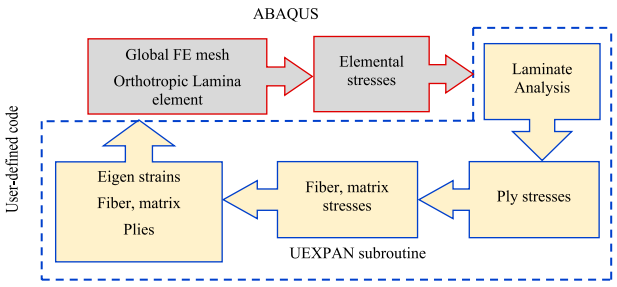

Figure 3. Processing stage scheme.

where

$$\boldsymbol{K}_{ij}^{m} = \int_{V_m} \left[\boldsymbol{A}_i^{m}\right]^T \boldsymbol{L}_m \boldsymbol{A}_j^{m}\, dV_m. \tag{23}$$

$$\boldsymbol{f}_i^{m} = -\int_{V_m} \left[\boldsymbol{A}_i^{m}\right]^T \boldsymbol{L}_m \boldsymbol{\mu}_m dV_m\,. \tag{24}$$

where P is the number of nodes per element and $\boldsymbol{f}_i^{m}$ is the element nodal loads associated with the element eigenstrains.

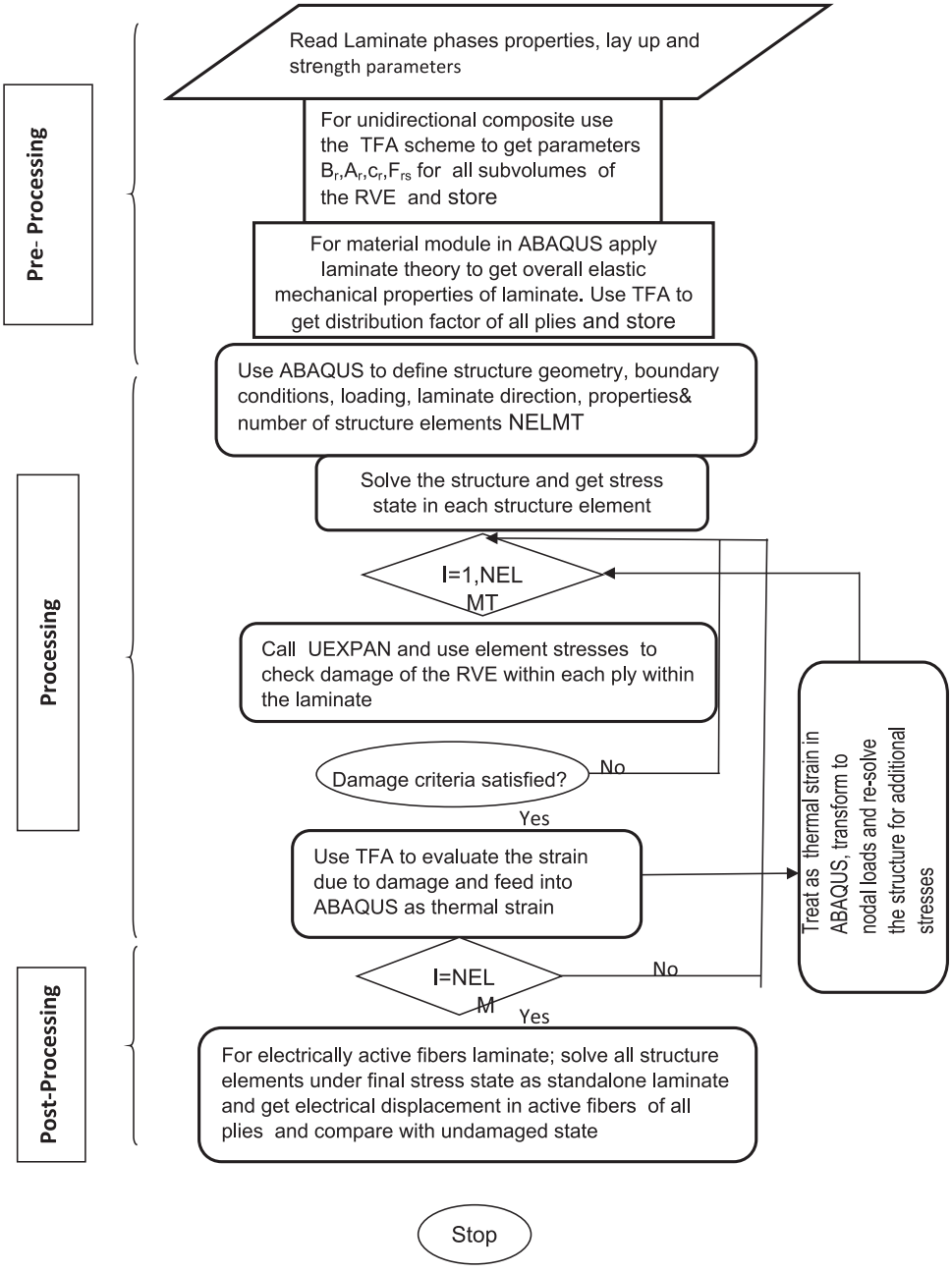

Figure 4. Schematic of solution technique.

To complete formulation, the sum of node i loads resulting from the elements stresses that share same node and the directly applied loads $\boldsymbol{p}_{\mathrm{i}}$ should vanish

$$\boldsymbol{p}_i - \sum_{m=1}^{M} \boldsymbol{q}_i^m = 0, \quad i = 1,2,...N. \tag{25}$$

where N is the total number of nodes in the domain. Substituting equation (24) into equation (25) the general set of equations of the domain V is written as

$$\sum_{m=1}^{M}\sum_{j=1}^{P} \boldsymbol{K}_{ij}^m \boldsymbol{a}_j^m = \boldsymbol{p}_i - \sum_{m=1}^{M} \boldsymbol{f}_i^m, \quad i = 1,2,...N. \tag{26}$$

or in an overall form

$$\boldsymbol{K}\boldsymbol{a} = \boldsymbol{f}, \; \boldsymbol{K}_{ij} = \sum_{m=1}^{M} \boldsymbol{K}_{ij}^m, \; \boldsymbol{f}_i = \boldsymbol{p}_i - \sum_{m=1}^{M} \boldsymbol{f}_i^m. \tag{27}$$

where $\boldsymbol{k}$ is the overall stiffness matrix, $\boldsymbol{f}$ is the vector of nodal loads and $\boldsymbol{a}$ is the nodal displacement vector. The stiffness matrix is therefore constant and depends on the material properties and the number and arrangement of the subvolumes V_m.

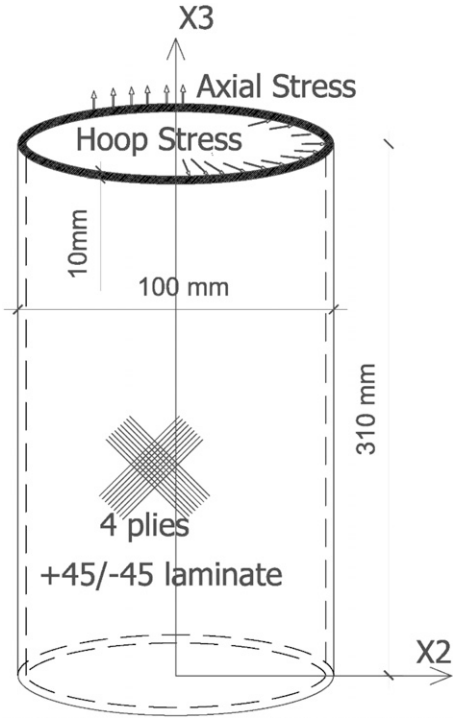

Figure 5. Geometry and dimensions of tested tube.

Damage analysis

Damage criteria

Checking damage is initiated at the composite micromechanical level denoted as the fiber/matrix interface debonding that may occur due to different failure modes. These modes include failure due to tension stresses perpendicular to the fiber/matrix interface or due to shear stresses in the hoop direction denoted as in-plane sliding or due to longitudinal shear parallel to fiber axis denoted as longitudinal shear sliding. The fiber/matrix interface elements stress vector is transformed from the composite coordinate system $(\overline{\mathbf{x}}_k, k = 1,2,3)$, Figure 1, to polar coordinate system (ξ,ω,Z) as shown in Figure 2. The failure criteria for debonding due to radial stresses can be written as follows

$$\overline{\sigma}_{\zeta\zeta}^r = \sigma_{\boldsymbol{u}T}^r. \tag{28}$$

And for longitudinal sliding

$$\left|\tau_{\boldsymbol{L}}^{\max}\right| + \mu_{\boldsymbol{L}}\langle\sigma_{\zeta\zeta}\rangle \geq \tau_{\boldsymbol{u}lt}, \; \tau_{\boldsymbol{L}} = \sqrt{\widehat{\sigma}_{23}^2 + \widehat{\sigma}_{31}^2}. \tag{29}$$

And for transverse sliding

$$|\sigma_{\zeta\omega}| + \mu_T\langle\sigma_{\zeta\zeta}\rangle \geq \tau_{\boldsymbol{u}lt}. \tag{30}$$

where $\sigma_{\boldsymbol{u}T}^r$ and τ_{ult} are the ultimate strength of the interface material in tension and shear, respectively. μ_T,$\mu_{\boldsymbol{L}}$ are the coefficients of friction for interface slippage in the transverse and longitudinal directions, respectively, and $\langle\mathbf{x}\rangle = \mathbf{x}$ if $\mathbf{x} < 0$, $\langle\mathbf{x}\rangle = 0$ if $\mathbf{x} \geq 0$.

If damage criteria are satisfied in any direction, the stresses in the failed directions should be set to zero. This can be done by applying additional unknown eigenstresses in the failed elements that when combined with the undamaged stress field, the stresses in the failed directions vanish. From equations (2) and (14), the following equation can be written for the stress field in any failed element r in ply i

$$\boldsymbol{\sigma}_r^i = \boldsymbol{B}_r\overline{\boldsymbol{\sigma}}_{undamaged} + \boldsymbol{B}_r\sum_{j=1,n}\boldsymbol{U}_{ij}\sum_{s=1,Q}\left(c_s\mathbf{A}_{\mathbf{s}}^{\mathbf{T}}\boldsymbol{\lambda}_s^{damaged}\right)^j + \sum_{s=1,Q}\mathbf{F}_{rs}\boldsymbol{\lambda}_s^i. \tag{31}$$

Table 1. Mechanical properties of tube problem constituents.[36]

Material	E [GPa]	ν	G [GPa]	σ ult [MPa]	σ ult [MPa]
Silenka E-glass	70	0.2	30.8	2150	—
MY750/HY917/DY063	3.35	0.35	1.24	80[a]	70[a]

[a]Material bulk strength.

The left-hand side of equation (31) is the final stress in subvolume r such that some components, or all of its components, should be set to zero. The first term in the right-hand side is the stress state in subvolume r under mechanical loads in the undamaged state which is known. The second and third terms in the right-hand side contain the unknown eignstresses $\boldsymbol{\lambda}_s$ that need to be determined and superimposed to satisfy the condition of vanishing final stress components. Rearranging the terms that contain the unknown eignstresses and solving equation (31), the eignstresses in all elements in all plies that exhibit failure can be obtained. The laminate eignstresses $\boldsymbol{f}'$ can be obtained using equations (7) and (13) and therefore the laminate overall strain $\boldsymbol{\varepsilon}_o$ is available using equation (12).

Sensing damage

Electro-mechanical coupling in piezoelectric fibers is a useful phenomenon to be employed for sensing damage and structural integrity interrogation. If any piezoelectric phase r exhibits a stress or strain vector $\boldsymbol{\sigma}_r/\boldsymbol{\varepsilon}_r$, the resulting electric displacement $\boldsymbol{D}_r$ in this phase can be expressed as follows[28]

$$\boldsymbol{D}_r = \boldsymbol{e}\boldsymbol{\varepsilon}_r = \boldsymbol{d}\boldsymbol{\sigma}_r. \tag{32}$$

where $\boldsymbol{e}_r$ and $\boldsymbol{d}_r$ are the material piezoelectric stress/strain coefficient matrices of phase r, respectively. They have the form

$$\boldsymbol{d}^{\mathrm{T}} = \begin{bmatrix} 0 & 0 & d_{31} \\ 0 & 0 & d_{31} \\ 0 & 0 & d_{33} \\ 0 & d_{15} & 0 \\ d_{15} & 0 & 0 \\ 0 & 0 & 0 \end{bmatrix}, \quad \boldsymbol{e}^{\mathrm{T}} = \begin{bmatrix} 0 & 0 & e_{31} \\ 0 & 0 & e_{31} \\ 0 & 0 & e_{33} \\ 0 & e_{15} & 0 \\ e_{15} & 0 & 0 \\ 0 & 0 & 0 \end{bmatrix}. \tag{33}$$

They are connected to the mechanical properties in terms of Hill's moduli as follows[28]

$$e_{31} = 2kd_{31} + ld_{33}, e_{33} = 2ld_{31} + nd_{33}, e_{15} = pd_{15}. \tag{34}$$

For a composite laminated structure which includes electrically active fibers, if damage occurs, the stresses in these fibers will exhibit some deviation from the fully intact structure readings in terms of the electrical displacement $\boldsymbol{D}_r$. These updated values of $\boldsymbol{D}_r$ can be used as flags to the degree of the integrity of the structure.

Solution strategy

In this section, the technique to combine the analysis of the three tiers during damage in one scheme is presented. The solution procedure can be divided into three stages: pre-processing stage, processing stage, and post-processing stage. In what follows, the tasks undertaken in each stage on each analysis scale are presented.

Figure 6. Stress σ_{33} for the (±45)s tube problem.

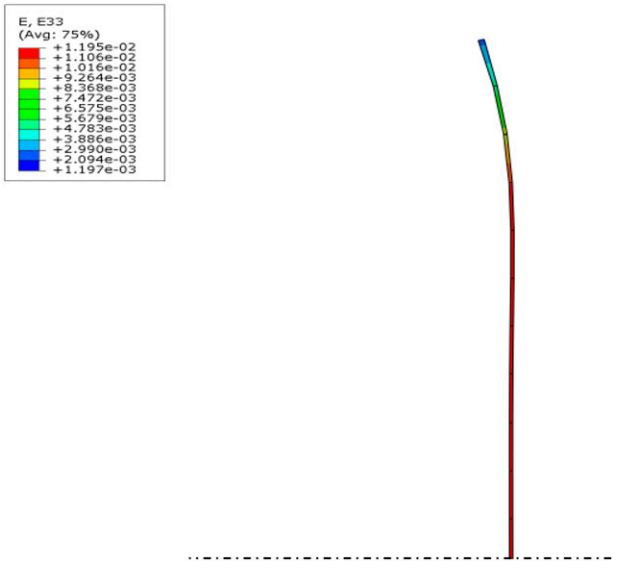

Figure 7. Strain E_{33} for the (±45)s tube problem.

Pre-processing stage

Composite level. Starting with the composite level, and for the specific discretization of the RVE, concentration factors of all elements and influence functions $\boldsymbol{A}_r$, $\boldsymbol{B}_r$ and $\boldsymbol{F}_{rs}$ are calculated using the FE. For the concentration factors, $\boldsymbol{A}_r$ and $\boldsymbol{B}_r$, the whole RVE is loaded with a unit stress in each direction in turn and the resulting 6 x 1 element stress vector represents one column in the 6 x 6 stress concentration factor for r subvolume $\boldsymbol{B}_r$. The strain concentration factor $\boldsymbol{A}_r$ can be obtained using equation (3). For the influence function $\boldsymbol{F}_{rs}$, equation (2), each element r in the RVE should be loaded with a unit stress in each direction in turn. The resulting stress vector in another element s represents one column in $\boldsymbol{F}_{rs}$. A certain criterion should be set to assess the weight of interactive influence between elements to avoid huge storage. It has to be noted that the stress/strain concentration factors and influence functions depend only on geometry, fiber volume fraction, and phase elastic properties.

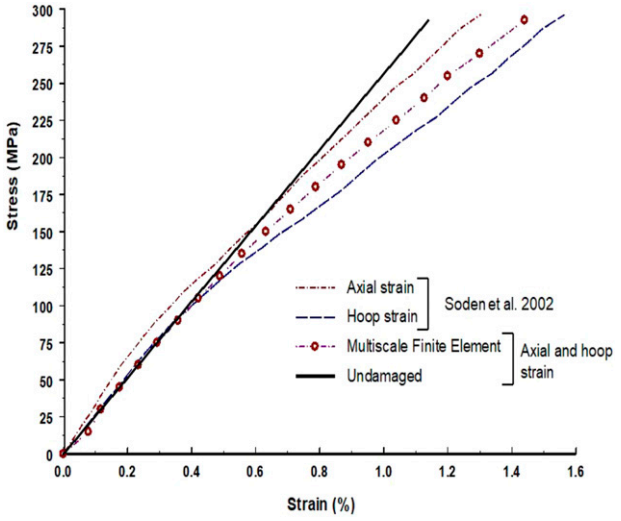

Figure 8. Axial and hoop stress-strain relationship for a (±45)s tube.

Laminate level. In this stage, the properties of the stress-free laminate are obtained. These properties include longitudinal Young's modulus, transverse Young's modulus, Poisson's ratio, and shear modulus. The laminate is solved using a standalone routine applying the conventional lamination theory under three in plane stresses in turn. Knowing the resulting strains, the overall properties of the laminate can be obtained. These properties depend only on laminate layup, plies' thickness, fibers volume fraction, and materials' properties. The resulting moduli will be induced as material properties in the FE package ABAQUS for structure level of analysis. In addition, the plies distribution factor for in-plane stresses $\boldsymbol{P}_i$, $i = 1, n$ where n is the number of plies, has to be obtained using equation (14) and stored. This can be done by applying a unit stress vector on the laminate in each direction in turn and the resulting ply stresses represent a column in the plies distribution factor $\boldsymbol{P}_i$.

Structure level. In ABAQUS, the user material is an orthotropic lamina and its properties are pre-prepared in the laminate pre-processing stage previously mentioned. The problem is defined as a thermos-mechanical problem where the thermal conductivity of the material is a user defined value prepared in the user routine UEXPAN. The thermal

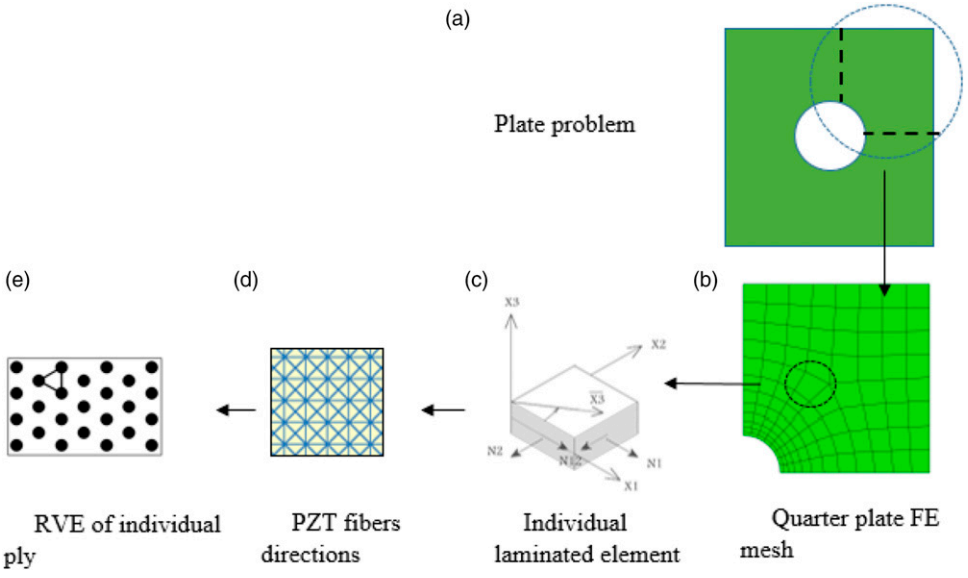

Figure 9. Progression of analysis of the plate with a hole problem.

strain to be calculated is actually the damage strains that occur in any structure element.

Processing stage

The processing stage starts with the structure level. The structure is solved under a predefined loading regime using ABAQUS in a thermomechanical step and the elements stresses are obtained. These stresses are used as input for UEXPAN user subroutine to check for damage in each structure element, which is eventually a symmetric laminate with n plies. In UEXPAN the other two tiers stress/strain fields are processed. For each structure element, and in UEXPAN, the individual ply i stresses within this element can be evaluated using equation (14). Then, the phase element r stresses are evaluated using equation (2). The element stress concentration factor $\boldsymbol{B}_r$ needed for applying equation (2) is prepared and stored in the preprocessing stage. Check for interface element failure using failure criteria equations (28)–(30) is to be performed to identify the damaged elements and the failed directions. Then, equation (31) can be applied to find the eignstresses in all failed elements due to damage. Using equations (9), (12), and (13), laminate mid plane strain due to the current damage state can be evaluated, which represents the "thermal" strains to be applied back on the structure element. ABAQUS will update the structure element strains and stresses to account for the additional "thermal" strains and re-check for more failure at same load level until damage saturation is attained. The flow of the fields between the different scales in the processing stage is shown in Figure 3.

Post-processing stage

Upon completion of the thermo-mechanical loading step in the processing stage, ABAQUS output element stresses can be used as input for a standalone electrically active laminate analysis. Using equation (32), the electric displacement vector $\boldsymbol{D}_r$ due to the current stress state can be calculated and compared with the undamaged electric displacement vector to assess the effect of damage on the electric response of the embedded electrically active fibers in the laminate. A schematic of the three-stage process and fields flow is given in Figure 4.

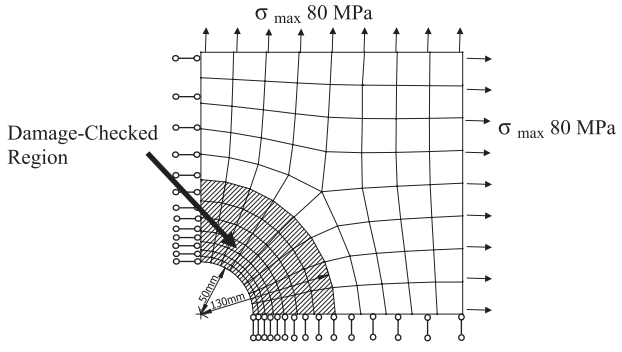

Figure 10. Geometry, boundary conditions and loading of a plate with a hole problem.

Application

Model verification

A test problem is performed to verify the above-mentioned strategy of tri-scale analysis. The results are compared with the experimental program conducted by Soden et al.[37] The test specimen is a tube with 300 mm length, 100 mm inner

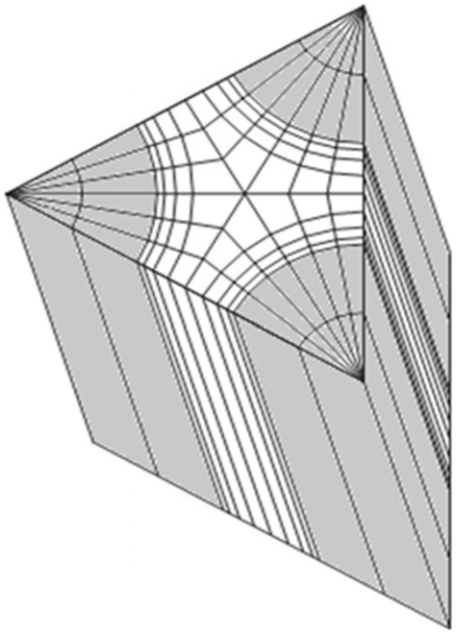

Figure 11. PHA 300 finite elements RVE.

Table 2. Mechanical properties of composite constituents.

Material	E [GPa]	ν	σ_{uT} [MPa]	σ_{uC} [MPa]	τ_u [MPa]
PZT-5A	60	0.34	1743	—	—
DY063 epoxy	3.35	0.35	31.72	115	46.36

Table 3. Electromechanical properties of PZT-5A fibers.

Material	$d*10^{-12}$ [m/V]		
PZT-5A	d_{31}	d_{33}	d_{51}
−171	347	584	

diameter and 1 mm thick as shown in Figure 5. The specimens were filament wound produced by QinetiQ. The tube layup is ±45 symmetric laminate. The fiber is Silenka E-glass with volume fraction 0.6 and the mechanical properties of the fibers are given in Table 1. The matrix is MY750/HY917/DY063 epoxy with the properties listed in Table 1. The curing cycle was 2 h at 90°C followed by 1.5 h at 130°C and 2 h at 150°C.[36] The tube is subjected to combined internal pressure and axial tension such that the ratio between the resulting hoop stress σ_θ and the axial stress σ_x is 1:1. The applied internal pressure $\boldsymbol{P}$ can be calculated from the relation

$$\sigma_\theta = \frac{\boldsymbol{PR}_i}{\boldsymbol{h}}. \tag{35}$$

Table 4. Mechanical properties of laminate.

Material	E_L [GPa]	E_T [GPa]	ν	G [GPa]
(0/±45/90)s	17.76	17.76	0.325	6.71

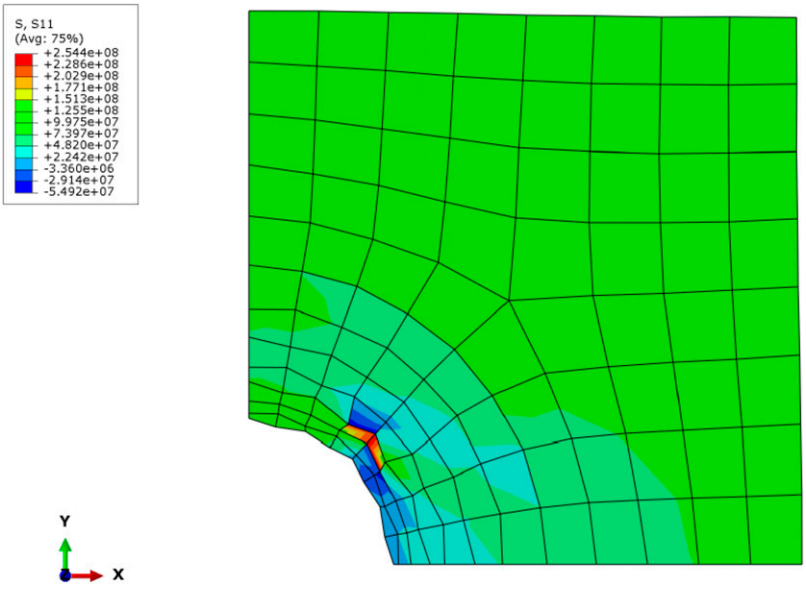

Figure 12. Stress distribution in *X* direction at applied stress 80 MPa.

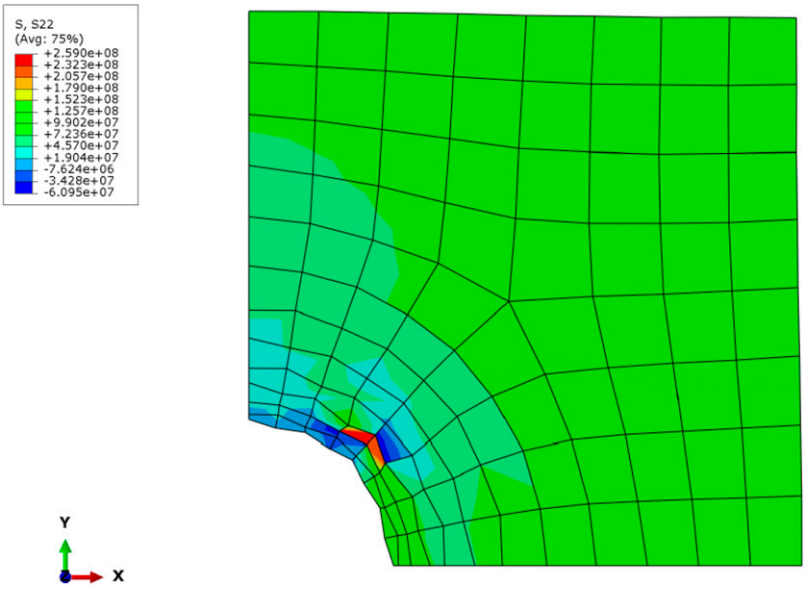

Figure 13. Stress distribution in *Y* direction at applied stress 80 MPa.

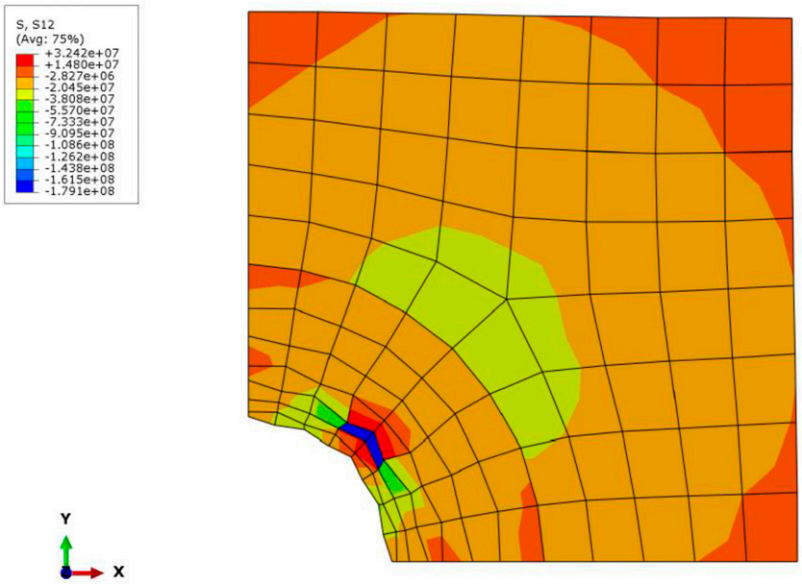

Figure 14. Stress distribution in *XY* direction at applied stress 80 MPa.

where $\boldsymbol{R}$ is the radius of the tube and $\boldsymbol{h}$ is the thickness. The axial force $\boldsymbol{F}$ can be obtained from the relation

$$\sigma_x = \frac{\boldsymbol{PR}_i}{2\boldsymbol{h}} + \frac{\boldsymbol{F}}{2\pi \boldsymbol{R}_i \boldsymbol{h}}. \quad (36)$$

In the pre-processing stage presented in *Pre-processing stage*, the $(\pm 45)_s$ laminate is analyzed using the TFA model for an undamaged state to find the overall elastic moduli of the laminate. The analysis results in laminate longitudinal and shear stiffness of 13.7 and 13.11 GPa, respectively. The tube is modelled in ABAQUS as an axisymmetric problem with 30 elements along the height of the tube. The necessary boundary conditions are added to account for tube fixation to grips. All the elements are checked against failure according to the failure criteria given in *Damage criteria*. The matrix tensile strength is taken as 100 MPa and shear strength of 87.5 MPa.[32] The interface strength is taken as 31.72 MPa, and the ultimate interface shear strength is taken as 46.36 MPa.[33] The stress and strain distribution along the length of the tube are presented in Figures 6 and 7. The stress–strain relation for the tube is given in Figure 8 compared with the experimental results retrieved from the work of Soden et al.[36] The undamaged plot is given for comparison. For the undamaged state, the results of the presented model are in good agreement with the experiment. As damage takes place and progresses, the model results lie between the experimental results for the hoop and the axial strains, which are naturally not identical due to the many factors that affect the readings.

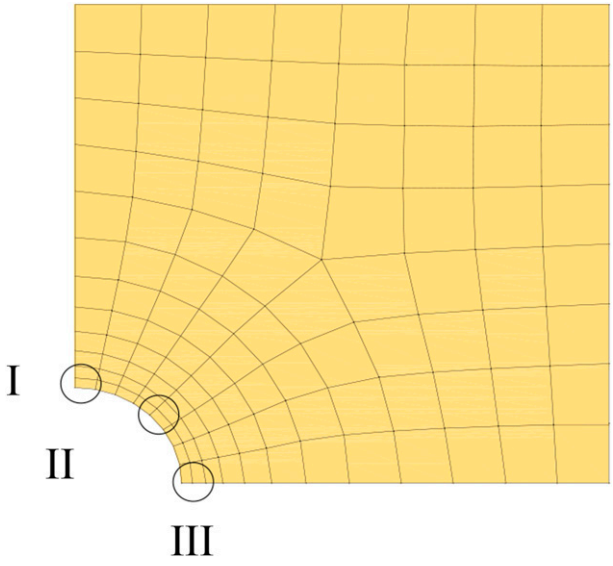

Figure 15. Locations for comparative values of stresses and electrical displacement.

Plate problem

Geometry. To investigate the capacity of the model to check the structure integrity, an electrically active square plate with dimensions 500 x 500 x 10 mm with central hole of diameter 100 mm under biaxial tension stress in global *X* and *Y* directions is solved. The plate material is a composite $(0/\pm 45/90)_s$ laminate. The fibers are electrically active with

volume fraction 0.55 for all plies. The three-tier analysis of the plate involves the plate level, the laminate level that represents the individual finite element within the plate, and the composite level that represents the individual ply. To reduce the problem size by employing the symmetry conditions, quarter of the plate is modeled and the appropriate boundary conditions are assigned to account for symmetry. A schematic of the progression of the analysis is shown in Figure 9. A circular region with diameter of 260 mm, where stress concentration due to the hole is assumed to affect the elements' stresses, is assigned for checking laminate damage as shown in Figure 10. The individual ply within each element is modeled using the Periodic Hexagonal Array model, PHA, with 300 finite elements per ply and using a refined element distribution near fiber matrix interface to account for the expected stress concentration. The 300 elements microstructure RVE of the PHA model is shown in Figure 11.

Materials. The composite phases employed in the plate with a hole problem are DY063 Epoxy for the matrix and electrically active PZT-5A fibers for all plies. Interface material properties are taken as the matrix material with longitudinal and transverse coefficients of friction depicted in equations (29) and (30), μ_L, μ_T , are 0.268. Mechanical properties of fibers and matrix are given in Table 2, while electromechanical properties of the PZT fiber found in equations (33) and (34), are given in Table 3. The standalone composite quasi-isotropic laminate is solved using the TFA model to find the overall moduli that will be used in the FE structure level analysis employing ABAQUS package. These properties are given in Table 4. In ABAQUS, the plate elements are modeled as orthotropic lamina with a user defined subroutine UEXPAN to find the thermal strains, which eventually are the damage strains.

Loads. Separate investigation on the standalone laminate level is conducted to figure out the applied stress at the onset of damage. Furthermore, in ABAQUS, and using the properties in Table 4, the stress concentration factor at 12 o'clock of the opening of the plate is investigated. Knowing both information, the loading path to be assigned to the structure can be designed to ensure damage would occur in different plies of the laminated structure elements. The selected loading regime is biaxial tension stress of 80 MPa in 8 increments.

Table 5. Element stresses at different locations for the undamaged and the damaged state.

	Undamaged element stresses at applied stress 80 MPa			Damaged element stresses at applied stress 80 MPa		
Location	S_{11} MPa	S_{22} MPa	S_{12} MPa	S_{11} MPa	S_{22} MPa	S_{12} MPa
I	122.78	7.0	−11.23	111.16	4.83	−7.43
II	77.73	52.38	−58	33.705	−22.33	11.42
III	7.0	122.78	−11.6	3.8	108.5	−5.91

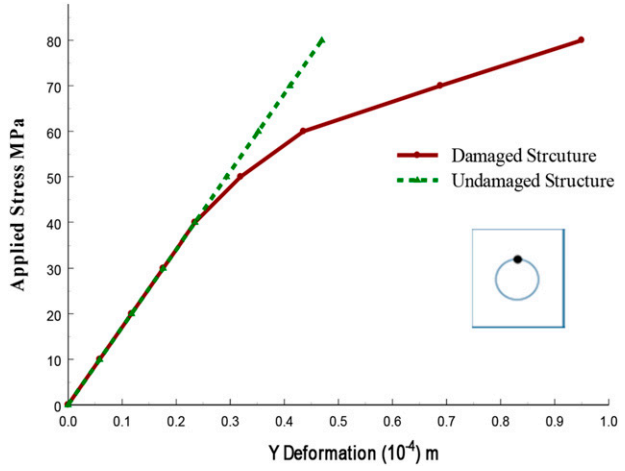

Figure 16. Stress-Deformation relationship at 12 o'clock of the opening.

Table 6. Electric displacement D_{33} for PZT fibers in all plies at different locations.

	D_{33} Undamaged at stress 80 MPa x10 [N/V.m]				D_{33} Damaged at stress 80 MPax10 [N/V.m]			
Location	0° ply	45° ply	−45° ply	90° ply	0° ply	45° ply	−45° ply	90° ply
I	0.9690	0.2210	0.4640	−0.2840	1.378	0.3528	0.6047	−0.4208
II	0.4803	−0.2839	0.9701	0.2058	0.5216	0.2403	−0.1461	−0.4274
III	−0.2836	0.2172	0.4680	0.9688	−0.4251	0.3661	0.5664	1.3576

(a)

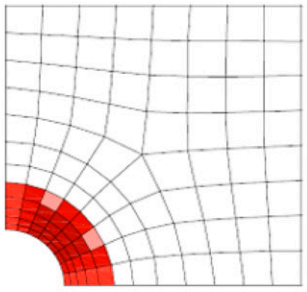

Damage level for the ±45° plies at stress 80 MPa.

(b)

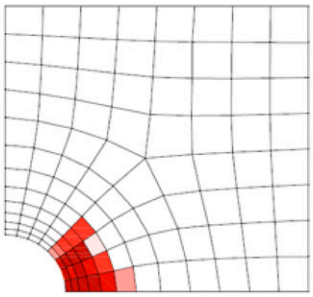

Damage level for the 0° plies at stress 80 MPa.

(c)

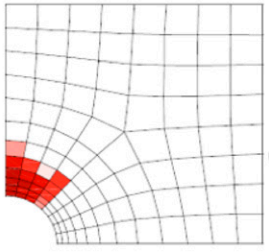

Damage level for the 90° plies at stress 80 MPa.

(d)

Angle φ	108°	96°	84°	48°	12°
Damage level					

Debonding angle at each damage level.

(e)

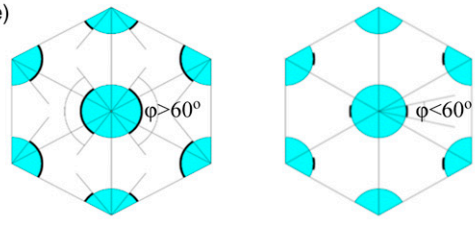

Failed arc of fiber/matrix interface.

Figure 17. Correlation between the state of damage and the debonding angle. (a) Damage level for the ±45° plies at load of 80 MPa. (b) Damage level for the 0° plies at load of 80 MPa. (c) Damage level for the 90° plies at load of 80 MPa. (d) Debonding angle at each damage level. (e) Failed arc of fiber/matrix interface.

Results. The stress distribution at the end of the loading path and after saturation of damage is shown in Figures 12– 14 for S_{11}, S_{22}, and S_{12}, respectively. To quantify the effect of damage on the stress field at different location in the plate, three points on the circumference of the hole are chosen. These points are denoted as I, II, and III as shown in Figure 15. Table 5 shows the stress field in the three locations I, II, and III at structure biaxial stress of 80 MPa if damage is taken into account compared to the undamaged case. The decrease in the load carrying capacity of the failed element in all direction is clear. The S_{11} stress at the tip of the opening reduced by 9% due to damage. The stress–deformation relationship at 12 o' clock of the opening is shown in Figure 16 for the undamaged and damaged state. The deviation from the undamaged state is clear where the opening significantly widens in both global X and Y directions if the damage of the laminate is taken into consideration compared to undamaged state.

The objective of the three-tier analysis of the plate is not limited to obtaining the overall or global behavior of the structure, but it is extended to interrogate the structure to identify the specific laminated element within the structure that suffers damage at a certain loading stage. Going deeply, the multi-scale scheme has the capacity to specify the ply within this element that exhibits damage and spotting the location and the nature of this damage. For example, for the plate problem, the onset of failure takes place at global biaxial tension stress of 40 MPa. The failure occurs in the first row of elements on the circumference of the opening, Figure 10. As loading continues, the failure progresses to other elements lying on farther circles. It has to be noted that the structure element failure may occur in various plies and due to different criteria according to the location of the element with respect to the opening circumference. The location of the element controls the nature of the stress field affecting this element. As an example, the elements at 45^{o} angle from the toe of the opening fail mainly in the $\pm 45^{o}$ plies satisfying the interface normal stress failure criteria, equation (28). This is attributed to the fact that these elements are subjected mainly to shear stresses. On the other hand, for the element at the 12 o'clock from the toe of the opening, the 90^{o} ply exhibits the most damage due to fiber/matrix debonding, equation (28). And vice versa, at the toe of the opening, the 0^{o} ply suffers the same mode of damage as the 90^{o} ply for the top element. The progression of failure in the plate at different locations and the affected plies within the laminates is shown in Figure 17. In this figure the correlation between the level of damage and the angle of fiber/matrix debonding is presented.

At the end of the loading stage, damage sensing can take place in the post-processing stage presented in *Post-processing stage*. For each structure element that suffers any stage of damage, the final stress field can be extracted from ABAQUS to be implemented in the post processing stage. Back to the standalone laminate analysis, the fiber stresses can be obtained from equation (2) and the electrical displacement D_{33} of the PZT fibers employed in all plies can be obtained using equation (32). At the end of the loading path, and for the selected locations in the plate structure shown in Figure 13, the electrical displacement D_{33} for the electrically active fibers is obtained and compared with the undamaged values. Summary of the results is given in Table 6. The increase in D_{33} of the fibers is attributed to the increase in fibers stresses as interface failure occurs and the load carrying capacity of the matrix is reduced. Example of this phenomenon is the electric displacement D_{33} of fibers at location I, Figure 15, where failure takes place primarily in the 90^{o} ply, the electric displacement in this ply increases due to interface failure with an angle of 108^{o}, Figure 17. Moreover, D_{33} of the fibers of the 0^{o} ply at the same location exhibits an increase of almost 50% for the load carrying capacity of the other plies is affected by failure. Same observation is applied for the off-axis plies where the direction of D_{33} is reversed due to the interface failure and hence a complex stress redistribution within the laminate.

Conclusion

A three-tier numerical scheme is used to check damage for the fiber reinforced composite structures. The scheme integrates different modelling regimes for each scale including the Transformation Field Analysis (TFA) for the non-mechanical fields in the composite phases, the laminate theory, and the Finite Elements for structure level. The three scales interact together and the fields flow from one scale to the other. Damage is detected in the micro-structure composite level and its effect on the overall laminate strains can be evaluated. The additional strains due to damage are treated as thermal stains in the failed elements of the structure level. Damage can be monitored by the increase in structure deformation and the change in the electrical response of the electrically active fibers embedded in the plies. Performing analysis on different scales enhances the understanding of the effect of inherent damage on the overall behavior of the structure. It also detects the cause of failure and assesses the integrity of the fiber/matrix interface bonding in all plies.

Declaration of conflicting interests

The author(s) declared no potential conflicts of interest with respect to the research, authorship, and/or publication of this article.

Funding

The author(s) received no financial support for the research, authorship, and/or publication of this article.

Data availability statement

The processed data required to reproduce these findings are available to download from https://www.sciencedirect.com/science/article/pii/S0266353802000933.

ORCID iD

Amany Micheal https://orcid.org/0000-0001-8241-6568

References

1. Aboudi J. Micromechanical analysis of fully coupled electro-magneto-thermo-elastic multiphase composites. *Smart Materials Structures J* 2001; 10: 867–877.
2. Berger H, Kari S, Gabbert U, et al. An analytical and numerical approach for calculating effective material coefficients of piezoelectric fiber composites. *Sol Structures Int J* 2005; 42: 5692–5714.
3. Berger H, Kari S, Bohn N, et al. A micro-macro approach to design active piezoelectric fiber composites. In: IUTAM Symposium on Mechanics and Reliability of Acting Materials, Beijing, China, 1–3 September 2004, pp. 121–130.
4. Chen T. Micromechanical estimates of the overall thermo-electroelastic moduli of multiphase fibrous composites. *Sol Structures Int J* 1994; 31(No. 22): 3099–3111.
5. Della NC and Shu D. On the performance of 1-3 piezoelectric composites with a passive and active matrix. *Sensors Actuators J* 2007; 140: 200–206.
6. Giurgiutiu V and Soutis C. Enhanced composite integrity through structural health monitoring. *Appl Compos Mater J* 2012; 19(5): 813–829.
7. Li X, Yang Z and Chen X. Quantitative damage detection and sparse sensor array optimization of carbon fiber reinforced resin composite laminates for wind turbine blades structure health monitoring. *Sensors J* 2014; 14: 7312–7331.
8. Medeiros R, Ribeiro ML and Tita V. Computational methodology of damage detection on composite cylinders, structural health monitoring for automotive components. *Automot Compos Int J* 2014; 1: 112–128.
9. Medeiros R, Sartorato M, Vandepitte D, et al. A comparative assessment of different frequency based damage detection in unidirectional composite plates using MFC sensors. *Sound Vib J* 2016; 383: 171–190.
10. Shivakumar J and Ray MC. Nonlinear analysis of smart cross-ply composite plates integrated with a distributed piezoelectric fiber reinforced composite actuators. *Adv Materials Structures J* 2008; 15: 40–52.
11. Cook CA and Senthil SV. Multiscale analysis of laminated plats with integrated piezoelectric fiber composite actuators. *Compos Structures J* 2012; 94: 322–336.
12. De Medeiros R, Lopes HMR, Guedes RM, et al. A new methodology for structural health monitoring applications. *Proc Eng* 2015; 114: 54–61.
13. Hwang H. Effect of the crack length on the piezoelectric damage monitoring of glass fiber epoxy composite DCB specimens. *Compos Sci Tech J* 2012; 72: 902–907.
14. Katunin A, Dragan K and Dziendzikowski M. Damage identification in aircraft composite structures, A case study using various non-destructuve testing techniques. *Compos Structures J* 2015; 127: 1–9.
15. Lissenden CJ, Blackshire JL and Puthillath PK. Structural health monitoring of composite laminates with embedded piezoelectric fibers. In: AIP Conference Proceedings, Chicago, Illinois, 3 March 2009 (1096(No. 1), pp. 974–981). College Park: American Institute of Physics.
16. Qing XP, Wang Y, Gao L, et al. Distributed multifunctional sensor network for composite structural state sensing. In: Proceedings of SPIE – The International Society for Optical Engineering, San Diego, California, 6 April 2012 (8345, pp. 83453O).
17. Stojic D, Nestorovic T and Markovic N. The application of piezoelectric transducers in the structure health monitoring of reinforced concrete structures. In: 12th International Multidisciplinary Scientific Geo Conference and Expo-Modern Management of Mine Producing, Geology and Environmental Protection, Albena, Bulgaria, 17–23 June 2012 (2, pp. 641–647).
18. Verijenko B and Verijenko V. A new structural health monitoring system for composite laminates. *Compos Structures J* 2005; 71: 315–319.
19. Bruner AJ, Barbezat M, Huber Ch, et al. The potential of active fiber composites made from piezoelectric fibers for actuating and sensing applications in structural health monitoring. *J Mater Structures* 2005; 38: 561–567.
20. Massarwa E, Aboudi J and Haj-Ali R. A multiscale modeling for failure predictions of fiber reinforced composite laminates. *J Composites B* 2019; 175: 107–166.
21. Dinha TD, Garoza D, Hajikazemia M, et al. Mesoscale analysis of ply-cracked composite laminates under in-plane and flexural thermo-mechanical loading. *J Composites Sci Tech* 2019; 175: 111–121.
22. Ren M, Cong J, Wang B, et al. Extended multiscale finite element method for small-deflection analysis of thin composite plates with aperiodic microstructure characteristics. *Composite Structures J* 2017; 160: 422–434.
23. Singh H, Gupta M and Mahajan P. Reduced order multiscale modeling of fiber reinforced polymer composites including plasticity and damage. *Mech Mater J* 2017; 111: 35–56.
24. Dvorak GJ. Transformation field analysis of inelastic composite. *Proc R Soc Lond* 1992; A437: 311–327.
25. Dvorak GJ and Benveniste Y. On transformation strains and uniform fields in multiphase elastic Media. *Proc R Soc Lond* 1992; 437: 291–310.
26. Bahei-El-Din YA and Botrous AG. Analysis of progressive fiber debonding in elastic laminates. *Int J Sol Structures* 2003; 40(25): 7035–7053.

27. Bahei-El-Din YA, Rajendran AM and Zikry MA. A micromechanical model for damage progression in woven composite systems. *Sol Structures J* 2004; 41(9–10): 2307–2330.
28. Bahei-El-Din YA. Modelling electromechanical coupling in woven composites exhibiting damage. *Proc Inst Mech Eng G, Aerospace Eng J* 2009; 223(5): 485–495.
29. Bahei-El-din YA and Micheal A. Micromechanical modelling of multifunctional composites. In: ASME International Mechanical Engineering Congress and Exposition Proceedings, Houston, TX, 9–15 November 2012, pp. 1329–1336. New York: ASME.
30. Bahei-El-Din Y and Micheal A. Multiscale analysis of multifunctional composite structures. In: ASME International Mechanical Engineering Congress and Exposition Proceedings, San Diego, CA, 15–21 November 2013, pp. 62427. New York: ASME.
31. Micheal AGB and Bahei-El-Din YA. Detecting laminate damage using embedded electrically active plies – An analytical approach. *Compos Structures J* 2017; 168: 772–779.
32. Bahei-El-Din YA and Micheal AGB. A multiscale model for damage progression and detection in piezo/pyroelectric composite laminates. *Mech Mater J* 2017; 113: 77–88.
33. Khire R, Bahei-El-Din YA and Hajela P. Multiscale transformation field analysis of progressive damage in fibrous laminates. *Multiscale Comput Eng J* 2010; 8(1): 69–80.
34. Zienkiewicz OC and Cormeau IC. Viscoplasticity-plasticity and creep in elastic solids- a unified numerical solution approach. *J Numer Methods Eng* 1974; 8: 821–845.
35. Bahei-El-Din YA. Finite element analysis of viscoplastic composite materials and structures. *Mech Compos Mater Structures J* 1996; 3: 1–28.
36. Soden PD, Hinton MJ and Kaddour AS. Biaxial test results for strength and deformation of a range of E-glass and carbon fibre reinforced composite laminates, failure exercise benchmark data. *Compos Sci Tech* 2002; 62: 1489–1514.